Estimates for secondary electron emission and desorption yields in grazing collisions of gold ions with beam pipes in the BNL Relativistic Heavy Ion Collider: Proposed mitigation

P. Thieberger,* W. Fischer, H. Hseuh, V. Ptitsyn, L. P. Snydstrup, D. Trbojevic, and S. Y. Zhang

C-A Department, Brookhaven National Laboratory, Upton, New York 11973, USA

(Received 29 June 2004; published 8 September 2004)

Grazing collisions with the stainless steel beam pipes of gold ions, the so-called "halo scraping," result in large secondary electron emission and surface molecular desorption yields in the Relativistic Heavy Ion Collider. Here we estimate electron emission yields as function of incidence angle, we show that desorption rates will follow a similar angular dependence at small angles, and we propose a simple approach to mitigate these effects.

DOI: 10.1103/PhysRevSTAB.7.093201 PACS numbers: 29.20.Dh, 29.20.Lq

I. INTRODUCTION

The purpose of this investigation is to estimate secondary electron and desorption yields due to heavy ion impacts on the Relativistic Heavy Ion Collider (RHIC) beam pipes to evaluate, and if possible mitigate, deleterious effects on the vacuum and on further electron multiplication due to multipacting.

Secondary electron yields (SEY) following heavy ion impact on solid surfaces have been studied for many years [1,2] over wide ranges of ion masses and energies. The yields have been shown to be approximately proportional to the energy loss per unit length (dE/dx), and inversely proportional to the sine of the angle of incidence. Here we take the angle of incidence to be the angle between the trajectory and its projection onto the surface. The more conventional definition of measuring incidence angles with respect to the normal to the surface is inconvenient for this application where we are mainly concerned with nearly grazing collisions, and where ion trajectories are referred to the beam axis, which is parallel to the beam pipe surfaces.

The conventional interpretation of the angular and dE/dx dependence of the secondary electron yield is schematically illustrated in Fig. 1. The larger the dE/dx value, the more electrons are created, and a fraction of these electrons will emerge, assuming they originate close enough to the surface. The part of the trajectory within this "escape depth" varies in length as $1/\sin(\alpha)$. Deviations from this angular dependence at small values of α are expected to be a consequence of multiple scattering, surface irregularities, beam energy loss, beam breakup, or a combination of some of these factors. Such deviations were observed during an experiment [3] in which 182 MeV gold, 126 MeV oxygen, and 28 MeV protons impinged on stainless steel surfaces at angles down to 0.7 mrad. While this angular range would be of interest for RHIC, the energy is vastly different. For gold the experiment was performed at ~0.9 MeV/amu while the RHIC injection energy is ~9 GeV/amu and the maximum energy is 100 GeV/amu.

Secondary electron yield measurements as a function of angle at such energies would be extremely difficult if very small incidence angles need to be reached. Clean beam collimation to better than ±0.5 mrad was required to obtain the gold results of Ref. [3]. While this is possible at 0.9 MeV/amu, it probably is not at 9 GeV/amu. In principle one could think of careful ion tracking and measuring electron yields from single ion impacts, but the associated effort and expense would be difficult to justify.

The approach followed here for secondary electrons was to assume that the semiempirical description mentioned above, which works well over many orders of magnitude at lower energies, can be extended by as many orders of magnitude towards higher energies. In addition, the qualitative arguments used so far [3] to explain small-angle deviations need to be incorporated quantitatively. This is not difficult to do since ion stopping, scattering, and breakup are fairly well understood and the surface topography can be measured.

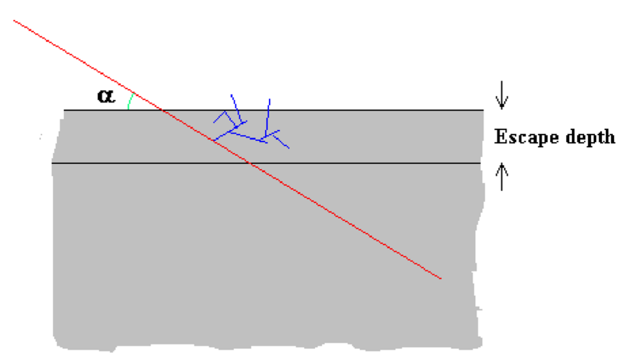

$$\text{Electron yield} \approx K \frac{dE}{dx} \frac{1}{\sin(\alpha)}$$

FIG. 1. (Color) Simple model for the angular and dE/dx dependence of secondary electron yields.

*Electronic address: PT@BNL.GOV

Ion impact molecular desorption yields are not very well understood at any energy even at normal incidence. The desorption yields also increase for smaller angles, but the angular dependence, down to a few degrees, is less pronounced than for secondary electrons [4]. However, we will show that for the very small angles of interest here, for RHIC energies, and for the considerable roughness of the RHIC beam pipe surface, both yields can be expected to have similar angular dependences. This happens because, at these grazing angles, the $\sim 1/\sin(\alpha)$ dependence for secondary electrons is no longer explained by the simple picture shown in Fig. 1, but by the fact that each ion enters and exits surface "corrugations" multiple times. It is now the number of these transitions that is proportional to $\sim 1/\sin(\alpha)$ and it determines both yields in a similar way. The deviations from the $1/\sin(\alpha)$ dependence due to multiple scattering and beam breakup will be essentially the same for both phenomena.

II. THE MONTE CARLO SIMULATION PROGRAM

To calculate expected electron yields as function of incidence angle we adopt the basic model illustrated in Fig. 1, but, due to multiple scattering, the ion trajectories will deviate from straight lines. We must also take into account that the ions lose energy thus changing their dE/dx and that, for high energies, the ions can break up. Finally, the surface can no longer be assumed to be flat.

Fairly reliable predictions of multiple scattering and energy loss up to ion energies close to 10 GeV/amu are provided by Ziegler's SRIM program [5]. Numerous theoretical refinements have been incorporated in this code over the years, and extensive comparisons with all available experimental data have been performed. Nuclear reactions do not occur for the first energy range we will consider below (0.9 MeV/amu). For the second energy range (9–100 GeV/amu), projectile breakup with geometric nuclear cross sections [6,7] will be the dominant nuclear process, and the only one taken into account. The fragments will make negligible contributions to the grazing incidence yields due to their smaller atomic numbers and their generally larger impact angles.

A Monte Carlo-type program was written which starts an ion trajectory above the surface with one of a sequence of incidence angles. It propagates the ion in steps small compared to the dimensions of the surface irregularities. For each step it determines what fraction, if any, of that segment is below the surface. It then determines what part, if any, of that fraction is close enough to the surface to emit electrons and it generates electrons in proportion to that part. The trajectory is continued until the ion stops, or the depth is too large for the ion to reemerge, or the ion is outside the surface moving away, or the ion breaks up. For each step or fraction of step inside the material, an appropriate stochastic energy loss and an appropriate stochastic scattering angle are applied, and in the case of high energies, the appropriate breakup probability is also applied.

The calculation described above is repeated several hundred times, then the next incidence angle is started, and so on. The results are normalized to the normal incidence yield that is either the measured value for the low energies, or that value scaled by the ratio of dE/dx values for the high energies. The scaling of the normal yield with dE/dx is well established over many orders of magnitude for lower energies [1,2] and it is part of the semiempirical model used here, where, after cascading, the number of generated electrons is proportional to the energy deposited by the ion.

The stochastic energy losses and scattering angles mentioned above are obtained from SRIM [5]. While in principle one could perform a SRIM calculation for each step, this would be hopelessly time consuming. Instead, lookup tables were generated with SRIM for a series of energies ranging from the initial beam energy down to a few percent of that value. The program retrieves values sequentially from the table that corresponds to the energy closest to the instantaneous energy of the ion. Each entry of a lookup table consists of a stochastic energy loss and a stochastic scattering angle calculated with SRIM for the given ion, the specified energy, and an appropriately chosen absorber thickness. Required scaling is performed when that absorber thickness does not coincide with the length of the trajectory segment for which the energy loss and scattering angle are being calculated. Namely, the energy loss is scaled with the ratio of lengths and the scattering angle with the square root of that ratio.

III. RESULTS FOR LOW ENERGIES AND COMPARISON WITH EXPERIMENTS

The Monte Carlo program was initially developed and tested with the experimental data [3] of 182 MeV gold ions impinging on a polished stainless steel surface. An example of ten trajectories generated by the program for 45° incidence is shown in Fig. 2. For the purpose of this illustration the trajectories were continued to a point close to the stopping point. We can see that multiple scattering effects become clearly visible after $\sim 2\ \mu$m of penetration. However, within the escape depth estimated to be ~ 10 Å for iron [8], these effects are totally negligible and therefore a $1/\sin(\alpha)$ angular dependence will result for these and even much smaller angles.

In contrast, for the three examples shown in Fig. 3, we see that at ~ 1 mrad incidence multiple scattering is very important. Surface irregularities were simulated through the superposition of three sinusoidal components of random phase and amplitudes randomly variable between zero and selected maximum values. The same type of

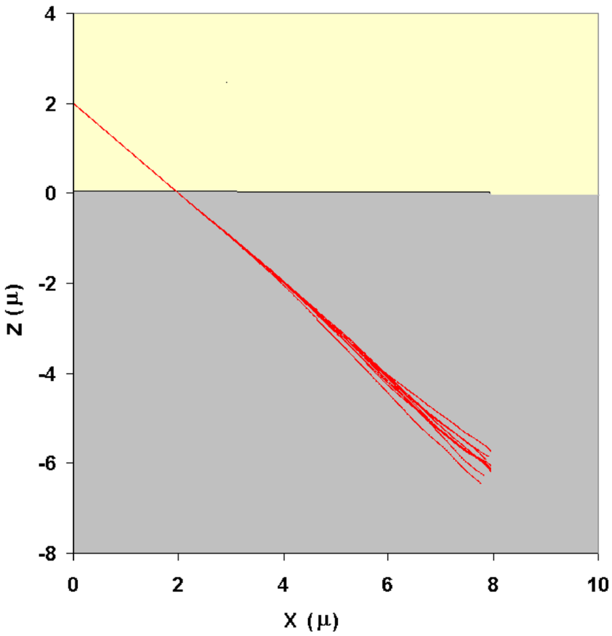

FIG. 2. (Color) Ten 182 MeV gold ion trajectories in iron generated with the Monte Carlo program for an incidence angle of 45°.

surface was used for the calculations of Fig. 2, but the irregularities are not visible there because of the very different vertical scale.

These simulated surfaces were also used for the electron yield calculations. Figure 4 shows the result for a simulation of the 182 MeV gold data [3].

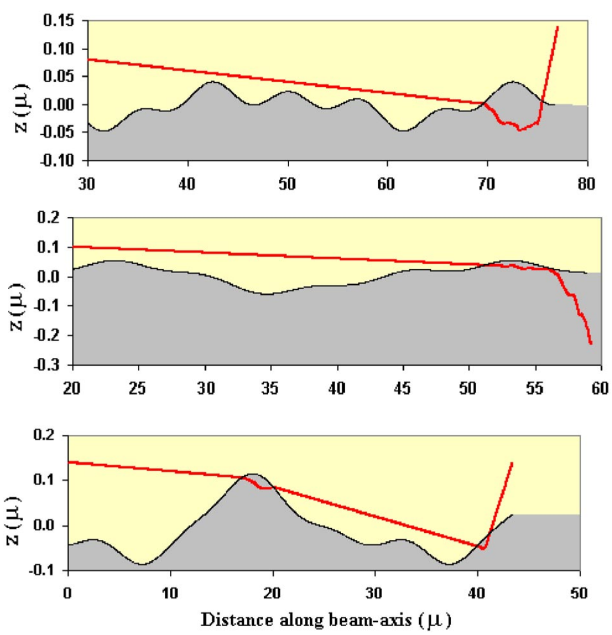

FIG. 3. (Color) Examples of near-grazing trajectories of 182 gold ions generated with the Monte Carlo simulation.

In this case the maximum peak-to-peak amplitude was 0.26 μm and the period of the fundamental was 30 μm. The actual topography of this polished stainless steel surface is unknown but these values are reasonable, and the simulation is not very sensitive to the particular values chosen for this "wavy" surface. In fact, even for a perfectly flat surface, while the fit is not good, we see that the essential feature of yield saturation for small angles is preserved.

IV. FIRST ESTIMATES OF ELECTRON YIELDS FOR GOLD BEAMS AT RHIC INJECTION ENERGY

The simulation for gold ions at the RHIC injection energy of 9 GeV/amu, and for the same surface waviness, is also shown in Fig. 4, taking into account that the dE/dx value is about 5 times smaller than at 0.9 MeV/amu. Compared to the relatively modest energy loss change from 0.9 to 9 GeV/amu, the other parameters that characterize these two beams are not even remotely similar. These large differences account for the very different angular dependences at small angles shown in Fig. 4. Table I lists these parameters.

Comparing these beams we see that the nuclear interaction length for the second one is so much larger than the range for the first one, and the scattering so much smaller, that it is not surprising to see its secondary electron yield continuing the $\sim 1/\sin(\alpha)$ behavior towards much smaller angles. But these calculations were performed for the same simulated surface topography corresponding to a well-polished material, and the interior surfaces of the RHIC warm beam pipes are not polished at all. It is therefore necessary to characterize their real topography before more accurate yield estimates can be made.

V. SURFACE TOPOGRAPHY OF THE RHIC WARM STAINLESS STEEL BEAM PIPES

Samples of a RHIC beam pipe wall were prepared and sent to Solarius Development Inc. [9] for surface mapping with one of their optical profilometers. The beam spot size used was 2 μm and a vertical resolution was 0.1 μm. Figure 5 shows an isometric view of a 1 mm $\times$ 1 mm area obtained with this instrument.

Another scan, this time of 50 mm $\times$ 0.2 mm, was performed to obtain numerical data on a 1 μm $\times$ 1 μm grid. Figure 6 shows one 50 mm long slice of this scan. Note that the vertical and horizontal scales differ by about 3 orders of magnitude. A small portion of the same data is shown in Fig. 7 without that distortion.

In the next sections we will evaluate the impact of the surface topography on the secondary electron and desorption yields.

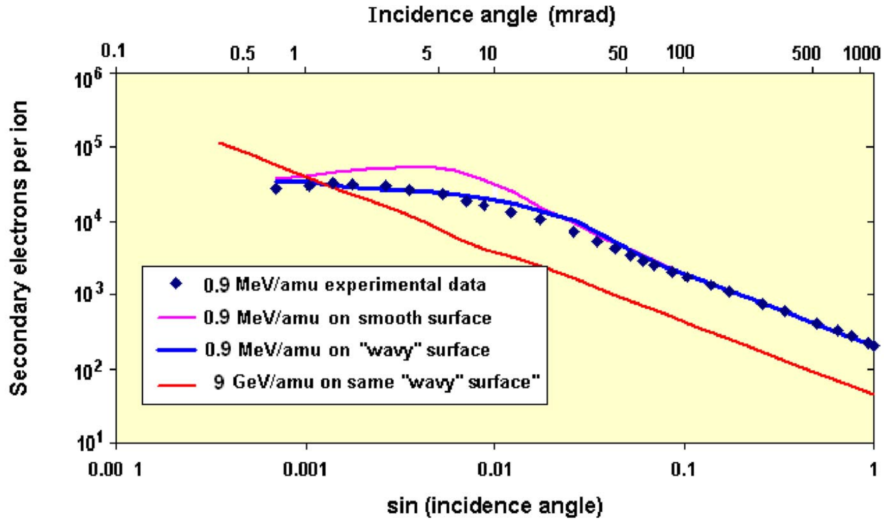

FIG. 4. (Color) 182 MeV gold on stainless steel secondary electron data and various results from simulations including one curve for 9 GeV/amu (see text).

TABLE I. Interaction of gold beams with iron at Tandem and RHIC injection energies.

Energy (MeV/amu)	Range (μm)	rms scattering angle in 1 μm of iron (mrad)	dE/dx [MeV/(mg/cm^2)]
0.9	8.3	17.9	50.1
9000	35 000[a]	0.0021	9.97

[a] This is the $1/e$ intensity point or "interaction length" due to nuclear breakup.

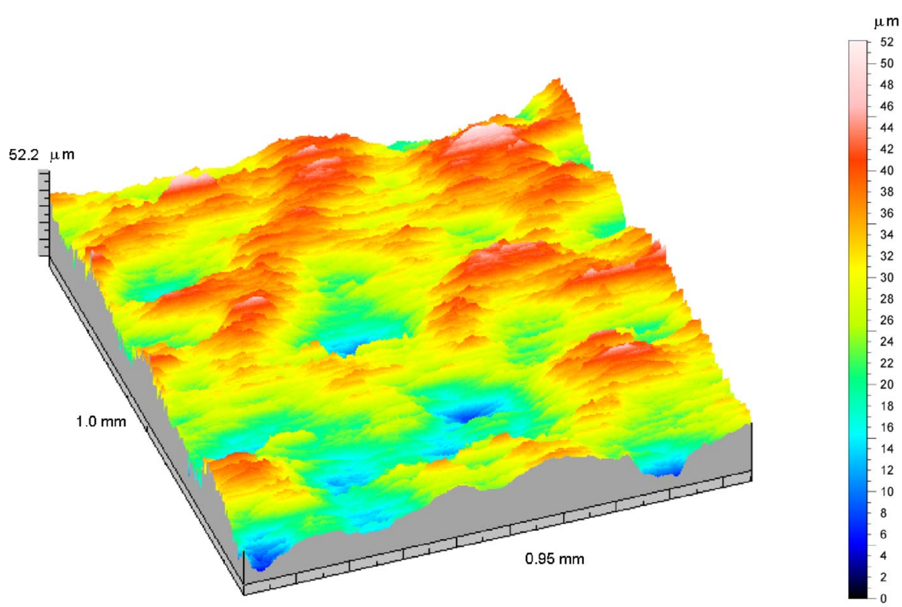

FIG. 5. (Color) Topographic view of a 1 mm × 1 mm portion of the interior surface of the RHIC beam pipe obtained by Solarius Development, Inc. [9] with one of their optical profilometers.

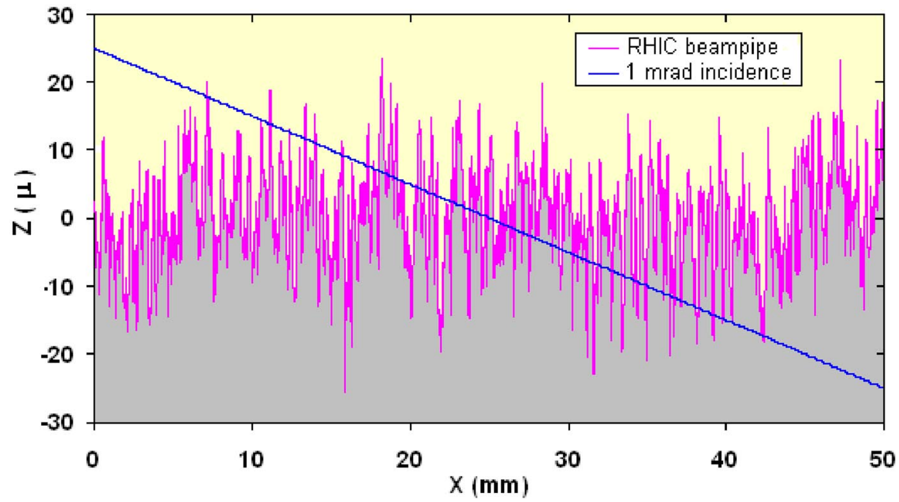

FIG. 6. (Color) Single slice of a 0.2 mm × 50 mm surface scan of RHIC beam pipe material obtained by Solarius, Inc. [9] using one of their optical profilometers. An ion trajectory incident at 1 mrad is superimposed, showing the multiple transitions between vacuum and solid.

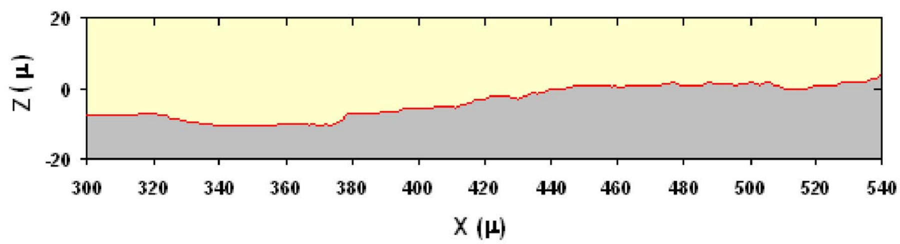

FIG. 7. (Color) Portion of the Fig. 6 RHIC beam pipe surface profile shown here with equal X and Z scales.

VI. SECONDARY ELECTRON YIELD ESTIMATES

We will now consider the impact of the surface topography results described in the previous section on the SEY. We could modify the Monte Carlo program to introduce measured profiles such as the one shown in Fig. 6 instead of the simulated surfaces described above. This has not been done yet. For the purposes of the present work it is easier and more instructive to perform a more limited and more transparent set of calculations using an Excel spreadsheet. The 50 000-point profile shown in Fig. 6 was thus analyzed in some detail.

Figure 8 shows the results of counting the transitions from vacuum to solid and solid to vacuum as the ion penetrates and exits the surface peaks. Figure 6 shows an example of such a trajectory, assumed to be a straight line, for a 1 mrad incidence angle. For the shallowest incidence angle shown in Fig. 8 (0.5 mrad) the total amount of steel traversed before the last transition (when the ion penetrates the solid without reemerging) is 21 mm, which corresponds to a SRIM-calculated rms scattering angle of 0.28 mrad and an energy loss of 8.4% . Therefore, to good approximation, we can ignore energy loss and multiple scattering effects for the range of incidence angles down to ~0.5 mrad analyzed here. In other words the assumption of straight line trajectories is justified, and the numbers of transitions plotted in Fig. 8 as function of incidence angle do not require significant corrections due to energy loss or multiple scattering.

There are, however, significant corrections due to gold ion breakup for the shallowest angles. For example only ~55% of the ions will actually survive to complete the number of transitions indicated by the solid point at 0.5 mrad incidence in Fig. 8. These corrections have been applied, and the corrected values are plotted as open circles in Fig. 8.

Secondary electrons are produced at each of the tens or hundreds of transitions discussed above. It is the number of these transitions as function of angle that determines the angular dependence of the SEY for incidence angles smaller than ~30 mrad for this surface. To confirm this, we plot the surface slope distribution and we see from Fig. 9 that the rms slope is ~140 mrad. Therefore changing the incidence angle by a few mrad will have very little effect on average yields from individual impacts.

The transition from the $N_o/\sin(\alpha)$ distribution due to the mechanism depicted in Fig. 1 and the same angular dependence for small angles due to multiple impacts is smooth and continuous. In fact, the constant N_o, which

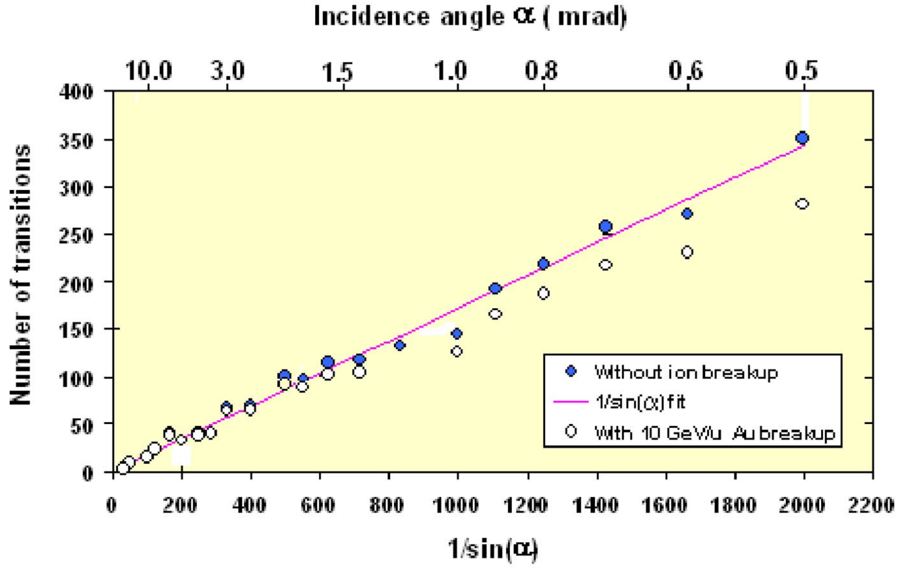

FIG. 8. (Color) Number of vacuum-solid and solid-vacuum transitions for an ion impinging on the surface characterized by the profile of Fig. 7 as function of incidence angle. These numbers corrected for gold ion breakup are also plotted.

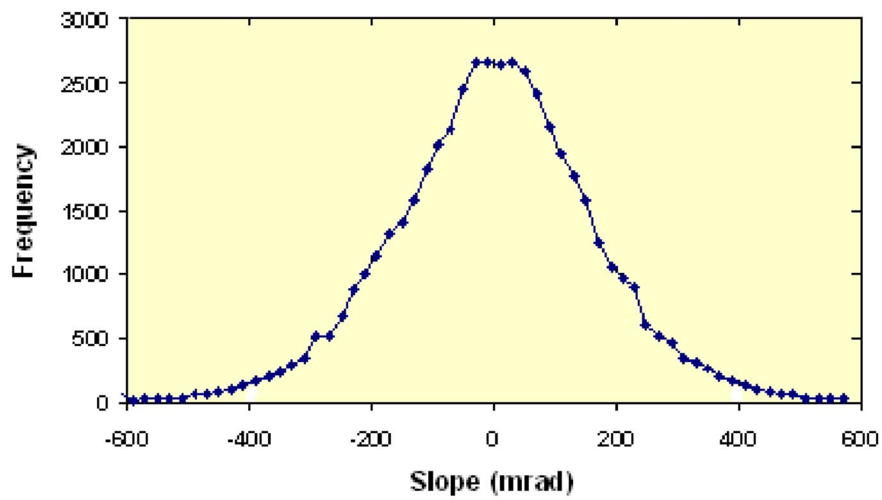

FIG. 9. (Color) Surface slope distribution for the RHIC beam pipe surface.

for the larger angles is defined as the SEY for normal incidence, changes very little between both regimes. This was shown analytically for protons impinging triangular serrations, which had been proposed [3] for the Spallation Neutron Source collimators. It is strictly true for shallow serrations when multiple scattering effects can be neglected. The same remarkable continuity was also observed here in the simulation of 9 GeV/amu interacting with a wavy surface (Fig. 4), where the transition occurs below a few mrad.

We conclude from these results that the RHIC beam pipe SEY for 9 GeV/amu gold impacts will closely follow the 9 GeV/amu line in Fig. 4 down to ~3 mrad and will then gradually deviate as indicated in Fig. 8. For example, for an incidence angle of 0.5 mrad the yield predicted in Fig. 8 is 80 000. This estimated yield is reduced to ~66 000 for the rougher RHIC beam pipe applying the correction indicated in Fig. 8. For even smaller angles, the SEY will continue increasing, but a complete simulation will be required to estimate by how much.

VII. DESORPTION YIELD ESTIMATES

Desorption yields also increase for smaller incidence angles [4] but the increase is not as pronounced. This angular dependence is not well understood. Recent extensive studies with 4.2 MeV/amu lead ions on differently treated and coated stainless steel surfaces [10] show yields around $\sim 10^4$ at normal incidence, little if any increase between normal incidence and 91 mrad, and a factor of ~2 increase between 91 and 14 mrad. Also a strong dependence on the charge state was demonstrated (a factor ~8 between 27+ and 53 +). It is difficult to extrapolate the measured results to different ions, energies, and charge states since there is not a good model or a good understanding for these dependencies.

For 10–100 GeV/amu gold in RHIC, perhaps the most relevant desorption data were recently obtained at the CERN Super Proton Synchroton (SPS) with a 158 GeV/amu In^{49+} beam incident at 35 mrad [11] with resulting desorption yields up to $\sim 10^5$. For a 79+ gold beam, the 35-mrad yield would probably be much higher in view of the above-mentioned charge-state dependence. Furthermore, at 35 mrad, we are at the beginning of the multi-impact regime for the RHIC beam pipe material (see Fig. 8). Individual impact and exit points are on average separated by over 10 μm, and will therefore make independent contributions to the desorption yield. As mentioned before, the total yield will therefore rise toward smaller angles with the number of impacts, i.e., with a $\sim 1/\sin(\alpha)$ dependence, limited only by the gradual onset of significant breakup and scattering below ~0.5 mrad. We can thus expect another factor ~30 when reaching 1 mrad. Thus starting with the indium data we reach estimated gold yields as high as $\sim 3 \times 10^6$, before taking into account the further likely increase due to a higher charge state. It is therefore reasonable to expect 1-mrad yields larger than 10^7.

VIII. PROPOSED MITIGATION

Besides applying low SEY coatings and using good cleaning and outgassing procedures, which is all being done at BNL [12], a next step to further reduce desorption and secondary electrons would be to reduce the number of very small angle impacts. One way to do this is to introduce annular ridges in the beam pipe to intercept halo ions before they can make grazing collisions with the walls. The impacts on the ridges would be mostly at large incidence angles generating little desorption and few secondary electrons. The ridges need to be long enough to stop or at least significantly scatter most ions.

Several triangular and rectangular cross section ridge configurations were studied. Figure 10 shows an example of such a rectangular ridge, which is close to what may be recommended for an actual test in one or two of the RHIC warm beam pipe sections.

In addition to the 10 mm thick ring shown in Fig. 10, 5 and 15 mm thick rings were also simulated, all with longitudinal spacings from one ring to the next of 2.5 and 5.0 m. For this purpose the Monte Carlo program was modified to accommodate these macroscopic shapes instead of simulations of the microscopic surface structure, and the step size used in the calculations was, by necessity, 1 mm instead of the 1 μm or less used before. The use of smooth surfaces in these simulations is well justi-

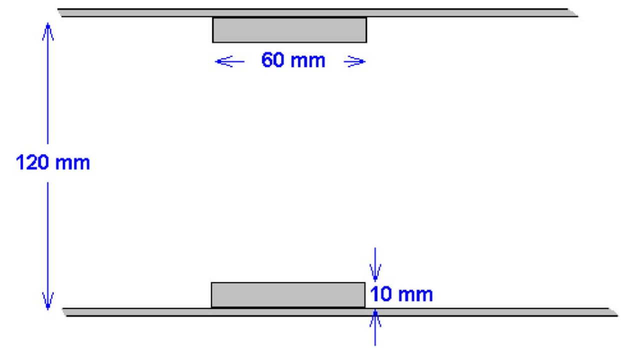

FIG. 10. (Color) Example of antigrazing ring placed in a section of RHIC beam pipe.

fied because, as we have shown above, for RHIC energies, surface roughness only starts significantly affecting the yield below ~1 mrad. With the proposed ridge configurations few if any ions will strike the beam pipe at such angles.

The results of the simulations are shown in Figs. 11 and 12. For the yield curve without ridges we show the ion-breakup correction obtained for the measured surface topography (see Fig. 8). Our use of planar instead of cylindrical geometry has a relatively minor impact on these results. As expected, for all the ridge configurations considered here we see considerable reductions in the secondary electron production. The small angle increases seen for all the configurations are due to secondary electrons from the ridge surfaces. Introducing a small angle in the ridge surface so as to avoid grazing collisions will largely eliminate this effect and increase the effectiveness of the ridges even further. This refinement will be adopted in the final design.

As discussed before, similar reductions in desorption yields can be expected. In fact, the improvements may be even greater since beam scrubbing, now mainly concentrated on the ridge surfaces, will be considerably accelerated.

A different way of reducing the number of small angle grazing collisions could be the slight intentional misalignment of beam pipe sections in a zigzag pattern. This approach was not analyzed in detail. It is clear, however, that this would be effective only if halo particles can be assumed to move away from the orbit staying, in their majority, close to the orbit plane.

Finally, it should be mentioned that our prediction of the deleterious impact of surface roughness on desorption yields is in agreement with experimental observations [13]. Polishing the interior surfaces of the beam pipes should therefore be considered as an additional possible mitigation technique. However, this approach may be in conflict with the observation [14] that rough surfaces reduce the secondary electron yield for electron impact, which is important for increasing the multipacting threshold. A solution may be the use of grooved surfaces

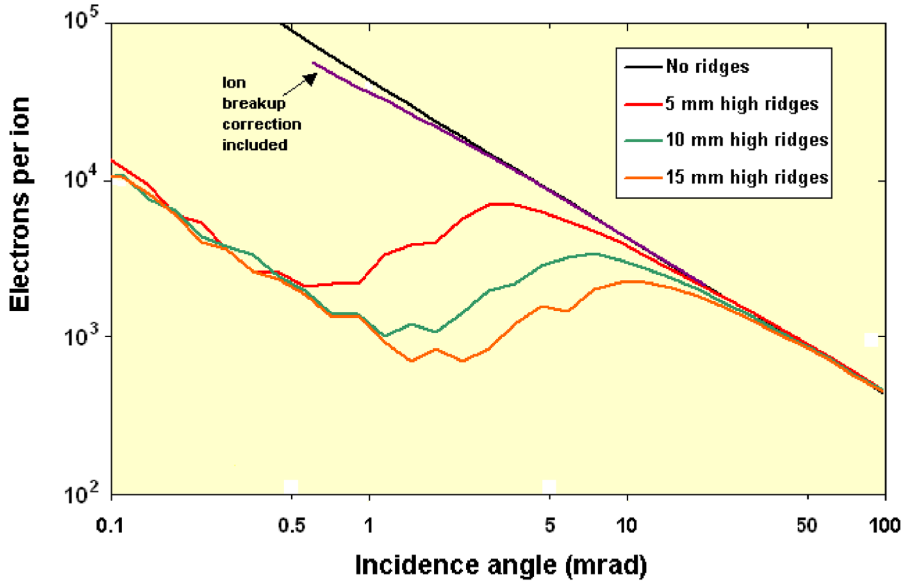

FIG. 11. (Color) Electron yields for 9.6 GeV/amu gold ions incident on stainless steel with ridges placed at 2.5 m intervals. Desorption rates will follow similar patterns.

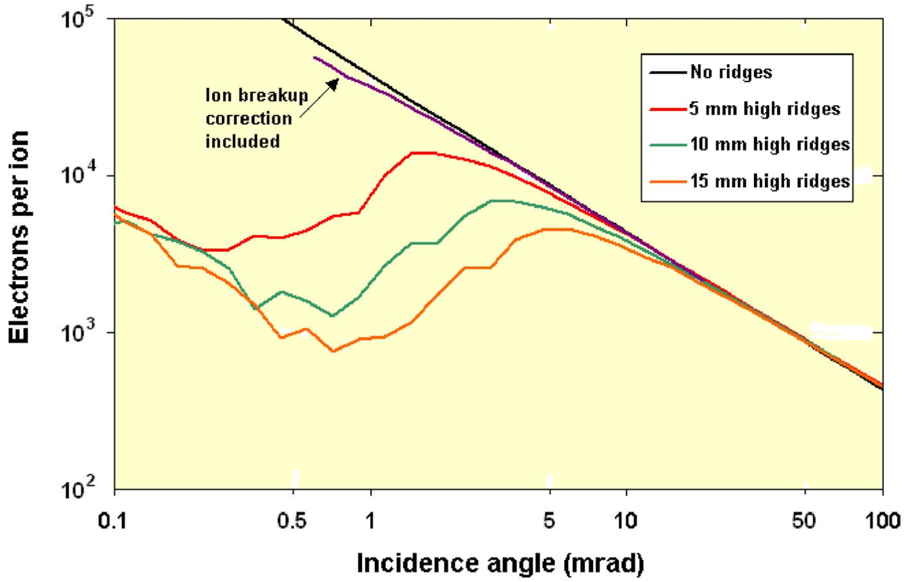

FIG. 12. (Color) Electron yields for 9.6 GeV/amu gold ions incident on stainless steel with ridges placed at 5 m intervals. Desorption rates will follow similar patterns.

[15], provided the grooves are parallel to the beam axis so as to minimize multiple ion entrance and exit transitions.

IX. OTHER DESIGN CONSIDERATIONS

The suggested introduction of "antigrazing" rings can have deleterious consequences unrelated to the intended results. Below we will briefly address possible issues related to reduced beam aperture, reduced pumping speed and impedance changes.

For the purpose of estimating the available aperture, we write the rms beam size in RHIC as

$$\sigma = \sqrt{\frac{\varepsilon_N \beta_{\mathrm{Twiss}}}{6\beta\gamma}},$$

where ε_N is the normalized emittance. In RHIC for gold ions $\varepsilon_N \approx 10$ mm mrad at injection, and up to $\varepsilon_N \approx 40$ mm mrad after hours at the store energy of 100 GeV/nucleon. The β_{Twiss} is the betatron function at the point of beam observation, while "$\beta\gamma$" is the relativistic factor. For gold $\beta\gamma = 108$ at the maximum energy and $\beta\gamma = 10.5$ at the injection energy.

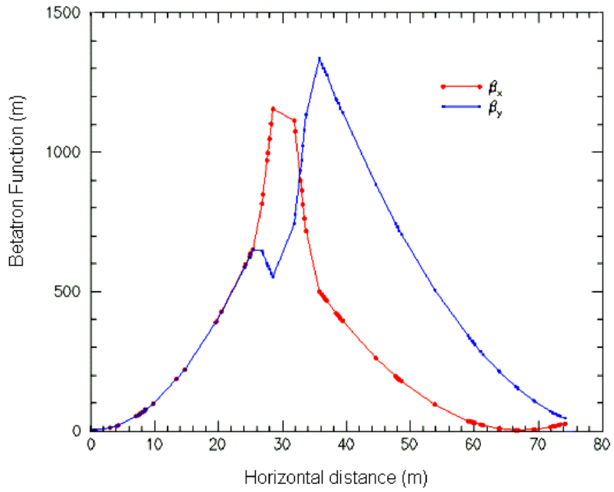

FIG. 13. (Color) The horizontal (β_x) and vertical (β_y) RHIC betatron functions starting at one of the collision points where the β function is 1 m. The warm section where antigrazing rings may be installed extends from the 38 m point to 74 m.

At injection, the maximum rms beam size in the drift areas where the antigrazing rings may be installed (see Fig. 13) is $\sigma \approx 4.6$ mm, with the maximum of the betatron functions of $\beta_x = 132$ m in the warm straight sections. At storage, the maximum rms beam size is $\sigma \approx 8.6$ mm with the maximum of the betatron function $\beta_x = 1189$ m in two of the interaction regions. In the other interaction regions the beam size at the location of interest is smaller.

The accepted rule for the minimum aperture size of the vacuum pipe in RHIC is that the inside diameter ID of the pipe is ID $\geq 12\sigma$. In a Gaussian profile, 3.3σ contain already 98% of the beam; however some margin is needed to account for orbit errors. The size of the beam pipe is ID $= 0.123$ m equal to 14σ at storage. If the 10 mm thick ring is inserted, the ID becomes 0.103 m, corresponding to 12σ of the beam size.

The effect of the antigrazing ring on the vacuum conductance of the 12 cm ID RHIC beam pipes has been evaluated for two cases: (1) 10 cm ID rings every 5 m, and (2) 9 cm ID rings every 2.5 m, which is the most severe case contemplated here in terms of aperture restriction. The reduction of the conductance from the pumps to the midpoint between two pumps, about 8 m away, is 7% for case (1) and 14% for case (2) as compared to that of no rings. The increase in average pressure due to the conductance loss will be approximately half of those percentages, and is insignificant compared with beam induced pressure rises.

For the purpose of impedance estimates, an antigrazing ring can be seen as an iris. Calculating the impedance of such an iris is reduced to two quasistatic problems, i.e., electrostatic and magnetostatic, and the associated impedance is inductive. The following parameters are used in the calculations: revolution frequency $\omega_0 = 2\pi \times 78 \times 10^3$ Hz, chamber radius $b = 0.06$ m, height of the ridge $h = 0.01$ m, and width $w = 0.06$ m. Usually, the longitudinal impedance per unit length, Z/n (where n is the mode or harmonic number), is used to evaluate the impedance contribution of a specific device or chamber modification. For one ring, we get $Z/n = 0.4$ mΩ. For six such rings in a straight section, the total impedance is simply $Z/n = 2.4$ mΩ, and if installed in the whole ring, the impedance is about $Z/n = 29$ mΩ, which is about 1.5% of the existing ring impedance. Once we decide to install such rings in the entire RHIC, then a $\sim 26°$ tapering of the ring edges could be applied to reduce the impedance by a factor of 2.

X. SUMMARY AND CONCLUSIONS

For a gold ion in RHIC, multiple impacts due to the surface roughness of the warm beam pipe will have little effect on the secondary electron yield down to a ~ 0.5 mrad incidence angle, but it will cause the desorption yield to also rise as $1/\sin(\alpha)$ for angles between ~ 30 and ~ 0.5 mrad. For even smaller angles, the rate of increase for the secondary electron and the desorption yields will both slow down, and eventually stop due to ion breakup and scattering, but at that point both yields will be large. Estimated lower limits for the maximum electron and desorption yields are 5×10^4 and $\sim 10^7$, respectively. Some macroscopic "roughness" is required to limit these yields to smaller values.

It has been shown in simulations that the suggested antigrazing rings can effectively reduce secondary electron and desorbed molecule production due to gold-beam halo scraping. The adverse impacts of such rings appear to be minor. The introduction of these rings should benefit collider operation to the extent to which such halo scraping effects are important. This question can be best answered by introducing the rings in some of the RHIC warm beam pipes.

ACKNOWLEDGMENTS

We are grateful for valuable suggestions and comments received from C. Chasman. This work performed under the auspices of the U.S. Department of Energy, Contract No. DE-AC02-98CH10886.

[1] M. Rvsler, W. Brauer, J. Devooght, J.-C. Dehaes, A. Dubus, M. Cailler, and J.-P. Ganachaud, *Particle Induced Electron Emission I*, edited by G. Hvhler and A. Niekisch, Springer Tracts Mod. Phys., Vol. 123 (Springer-Verlag, Berlin, 1991).
[2] H. Rothard, Scanning Microsc. **9**, 1 (1995).
[3] P. Thieberger, A. L Hanson, D. B. Steski, V. Zajic, S. Y. Zhang, and H. Ludewig, Phys. Rev. A **61**, 042901 (2000).

[4] A.W. Molvik, R. Cohen, A. Friedman, S. M. Lund, D. Baca, F. M. Bieniosek, M. Furman, E. P. Lee, L. R. Prost, P. A. Seidl, J.-L. Vay, and A. Sakumi, in *Proceedings of the Particle Accelerator Conference, Portland, OR, 2003* (IEEE, Piscataway, NJ, 2003), p. 312.
[5] J. F. Ziegler and J. P. Biersack, *The Stopping Power and Ranges of Ions in Matter* (Pergamon, New York, 1985); SRIM program (updated 2003 version), http://www.srim.org/SRIM/SRIMLEGL.htm.
[6] J. Stachel and G. R. Young, Annu. Rev. Nucl. Part. Sci. **42**, 537 (1992).
[7] Cheuk-Yin Wong, *Introduction to High-Energy Heavy-Ion Collisions* (World Scientific, Singapore, 1994), pp. 265—291, and references therein.
[8] M. Jung, H. Rothard, B. Gervais, Jean–Pierre Grandin, A. Clouvas, and Ralf Wünsch, Phys. Rev. A **54**, 4153 (1996).
[9] Solarius Development Inc., Sunnyvale, CA, USA.
[10] E. Mahner, J. Hansen, J.-M. Laurent, and N. Madsen, Phys. Rev. ST Accel. Beams **6**, 013201 (2003).
[11] E. Mahner *et al.*, in Proceedings of the European Particle Accelerator Conference, Lucerne, Switzerland, 2004 (to be published); in *Proceedings of the 13th ICFA Beam Dynamics Mini-Workshop, Brookhaven National Laboratory, Upton, NY, 2003*, http://www.cad.bnl.gov/icfa/agenda.html.
[12] P. He, H. C. Hseuh, R. C. Lee, M. Mapes, L. A. Smart, D. Weiss, and S. Y. Zhang, in *Proceedings of the Particle Acclerator Conference, Portland, OR, 2003* (Ref. [4]), p. 785.
[13] E. Mahner, J. Hansen, D. Küchler, M. Malabaila, and M. Tamborelli, CERN Divisional Report No. CERN AT/2003-6(VAC).
[14] H.C. Hseuh, in *Proceedings of the 13th ICFA Beam Dynamics Mini-Workshop, Brookhaven National Laboratory, Upton, NY, 2003* (Ref. [11]).
[15] G. Stupakov and M. Pivi, in *Proceedings of ECLOUD'04, Napa, CA, 2004*, http://mafurman.lbl.gov/ECLOUD04_proceedings.